Available online at www.sciencedirect.com
SCIENCE DIRECT
Journal of Nuclear Materials 347 (2005) 140–150
journal of nuclear materials
www.elsevier.com/locate/jnucmat

Phase boundary of the Zr-rich region in commercial grade Zr–Nb alloys

Hyun-Gil Kim, Jeong-Yong Park, Yong-Hwan Jeong *

Zirconium Fuel Cladding Team, Korea Atomic Energy Research Institute, P.O. Box 105, 150, Doekjin-dong, Yuseong-gu, Daejeon 305-353, Republic of Korea

Received 14 April 2005; accepted 9 August 2005

Abstract

The $\alpha/(\alpha+\beta)/\beta$ transformation temperature, the solubility limit of Nb, and the monotectoid temperature of the Zr–Nb binary system were investigated using commercial grade Zr containing 1400 ppm O and 700 ppm Fe and different Nb levels with a high purity. The microstructure characterization was carried out using OM, SEM and TEM and the phase transformation behavior was also investigated using DSC. From the microstructure examination using OM and SEM, it was revealded that the $(\alpha+\beta)$ region was expanded in commercial grade Zr containing 1400 ppm O and 700 ppm Fe. From the microstructure characterization using TEM, it was revealed that the Nb solubility in α-Zr of quaternary alloy was 0.2 wt%. And the monotectoid temperature of the commercial grade quaternary system of Zr, O, Fe, and Nb was revealed as 585 °C from the SEM, TEM and XRD analysis. The phase boundary of the Zr-rich region in a restricted quaternary alloy of Zr–0.14O–0.07Fe–*x*Nb system was established on the basis of the results obtained in this study using sponge-type Zr. The results of this study were largely different compared with results of the Zr–Nb binary alloy, however, these results could be used at the case of the Zr-rich corner of the phase diagram for a restricted quaternary alloy of Zr–0.14O–0.07Fe–*x*Nb system.

1. Introduction

The development of advanced cladding materials with an improved corrosion resistance has been widely carried out in many countries operating nuclear power plants for the last few decades [1–3]. Nb is an important alloying element in the advanced Zr-based alloys. Although a number of researches [1–6] were carried out to optimize the Nb content and annealing conditions in the Nb-containing Zr alloys, the optimum Nb content for a good corrosion resistance has been reported differently since the optimum Nb content for a corrosion resistance of the Nb-containing Zr alloys depended on the impurities which were assumed to change the Nb solubility and the monotectoid temperature in the alloy system. Therefore, it is essential to investigate the phase stability of the commercial grade Zr–Nb binary alloy system for developing advanced fuel

* Corresponding author. Tel.: +82 42 868 2322; fax: +82 42 862 0432.
E-mail address: yhjeong@kaeri.re.kr (Y.-H. Jeong).

0022-3115/$ - see front matter © 2005 Elsevier B.V. All rights reserved.
doi:10.1016/j.jnucmat.2005.08.008

cladding materials with a superior corrosion resistance. The phase diagram of the Zr–Nb binary alloy was extensively studied using iodide Zr and sponge type Zr [7–13]. For example, Lundin and Cox [7] reported that the α/β transformation temperature and the monotectoid temperature of Zr–Nb binary alloys were 863 °C and 610 °C, respectively, and the Nb solubility in α-Zr was 0.6 wt%. However, the commercial grade sponge-type Zr, which is actually being used in the manufacturing of the fuel cladding, contains O and Fe as impurities in the range of 10^2–10^3 ppm. Therefore, it is not reasonable to apply the previous results on the Zr–Nb phase stability directly to the heat treatment conditions for the development of advanced Zr-alloys.

In this study, the phase stability of the Zr–Nb alloy system was investigated using Zr containing 1400 ppm O which is the amount in most fuel claddings and 700 ppm Fe. The characterization of the microstructure and phase transformation was performed in order to establish the phase boundary in the Zr-rich region.

2. Experimental procedure

The chemical compositions of the Zr alloys used in this study are the Zr–xNb system ($x = 0$, 0.05, 0.1, 0.2, 0.3, 0.4, 0.5, 0.8, 1.0, 2.0 and 10.0 wt%). Nb of 99.9% and Zr containing 1400 ppm O which was additionally added to commercial grade sponge-type Zr and 700 ppm Fe were used for manufacturing the experimental alloys. Button ingots, ≈300 g, were prepared by an arc melting under an argon atmosphere and remelted at least

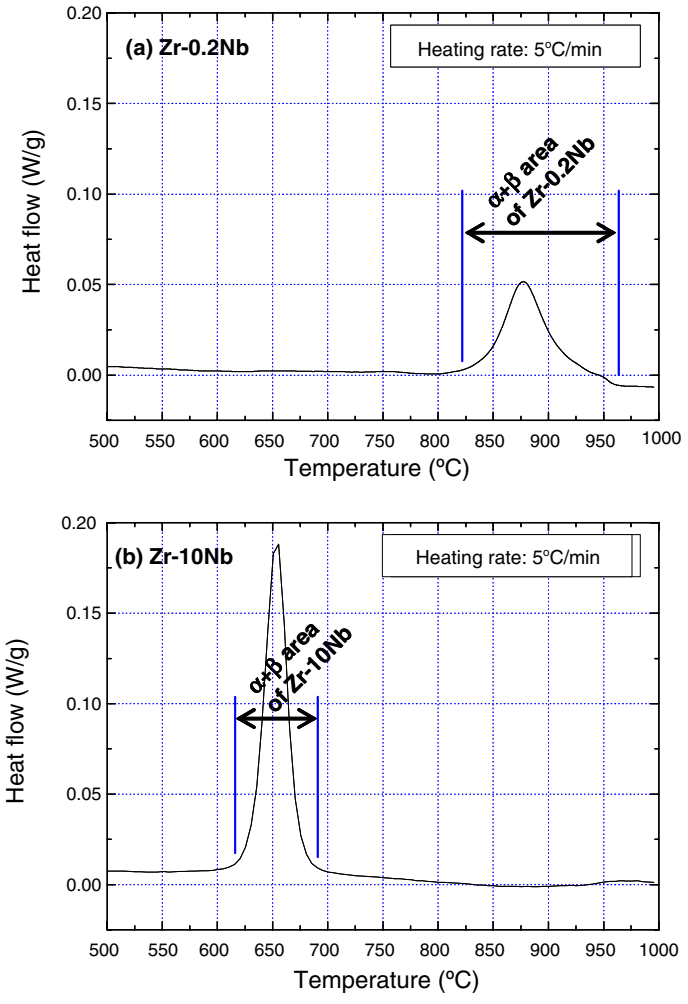

Fig. 1. DSC data of Zr–0.2Nb and Zr–10Nb alloys containing 1400 ppm O and 700 ppm Fe.

five times to promote the homogeneity of the as-cast structure. The arc-melted ingots were solution-treated at 1050 °C for 30 min in a vacuum furnace, hot-rolled after a pre-heating at 700 °C for 30 min, and cold-rolled three times to a final thickness of 1 mm. Between the rolling steps, the cold-rolled sheets were intermediately annealed at 600 °C in a vacuum furnace for 2 h to obtain the fully recrystallized structure. The final cold-rolled sheets were β-quenched in water with a cooling rate of about 1200 °C/sec from the temperature of 1050 °C, and then quenched in water after isothermally annealed at various temperatures for a long time to reach the equilibrium phase from 3 h to 3 months. Transformation temperatures of Zr–Nb alloys with low Nb contents were measured by using DSC in an Ar atmosphere. The microstructures of the alloys were examined using OM, SEM, and TEM equipped with an EDS. The TEM specimens were prepared by a twin-jet polisher with a solution of 10 vol.% $HClO_3$ and 90 vol.% C_2H_5OH after a mechanical thinning to 70 μm.

3. Results and discussion

3.1. The α/(α + β) and (α + β)/β phase boundary in Zr-rich region

The phase boundary in the Zr–Nb alloy was inevitably affected by the impurities [14]. The oxygen which is known as one of the α stabilizing elements in the Zr–Nb alloy is considered to be the most important element in terms of the phase stability [15]. As a preliminary study for selecting the annealing temperature for the microstructure characterization, the phase boundary and the Nb solubility in α-Zr in the quaternary Zr-rich region were examined by DSC. From the DSC results of Fig. 1, the phase boundary of the α/(α + β) and (α + β)/β transus lines were observed in the Zr–0.2Nb and Zr–10.0Nb alloys which contained 1400 ppm O and 700 ppm Fe. The α/(α + β) and (α + β)/β transus temperature ranges of the Zr–0.2Nb alloy were roughly showed from 820 °C to 970 °C and those of the Zr–10Nb alloy were roughly showed from 620 °C to 680 °C. The starting and finishing

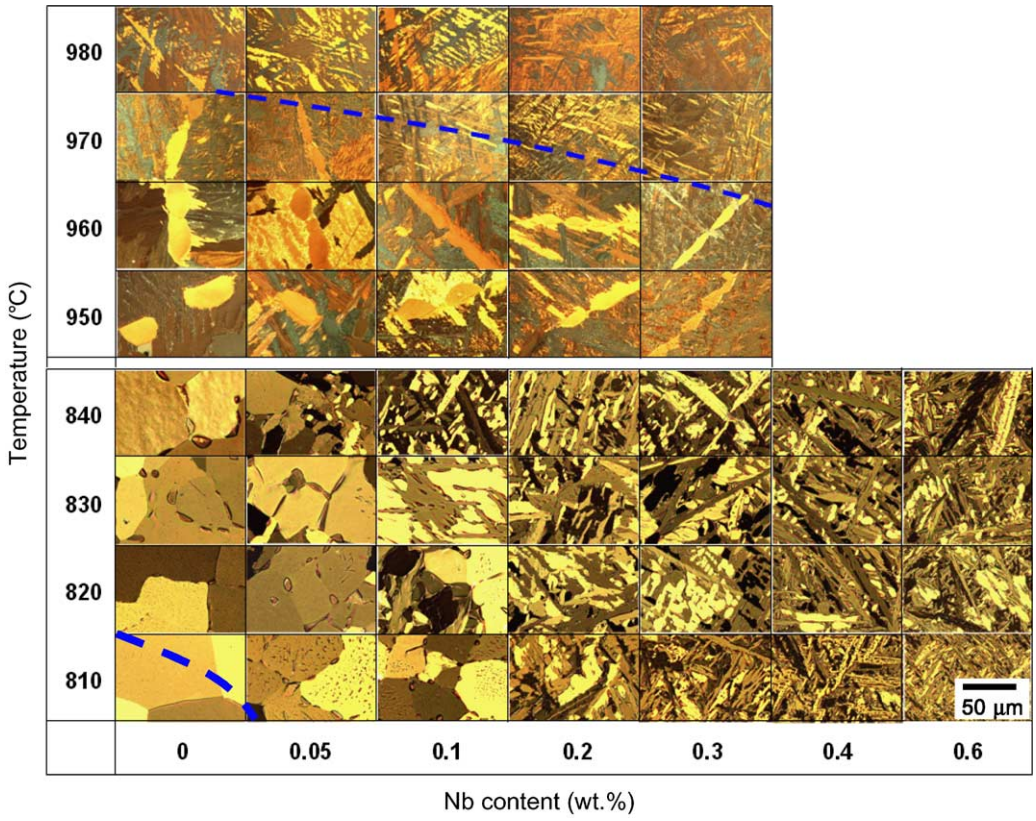

Fig. 2. Optical micrographs of Zr–*x*Nb alloys annealed at the various temperatures for different annealing time between 3 and 24 h.

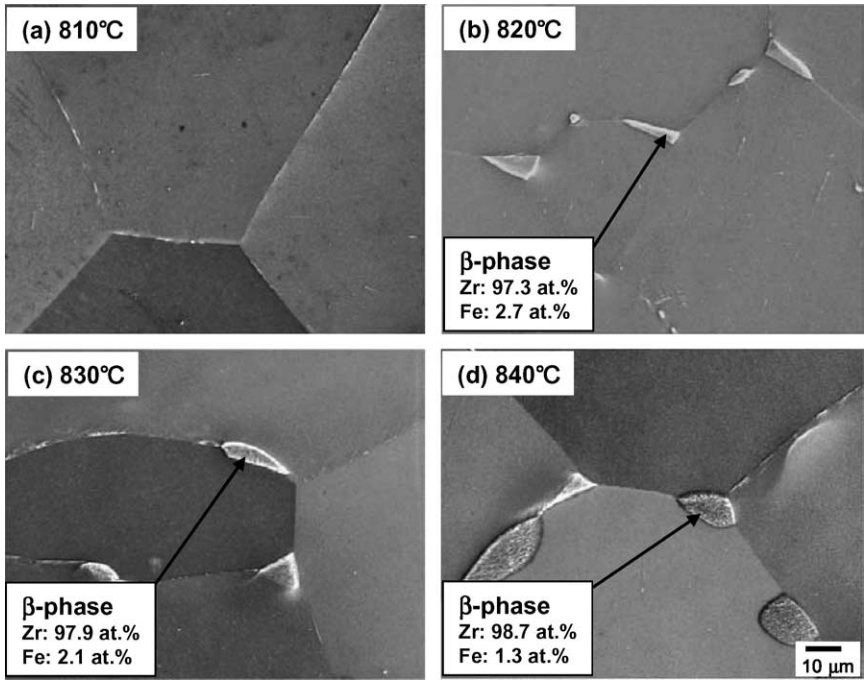

Fig. 3. SEM micrographs of sponge Zr containing 1400 ppm O and 700 ppm Fe with different annealing temperature.

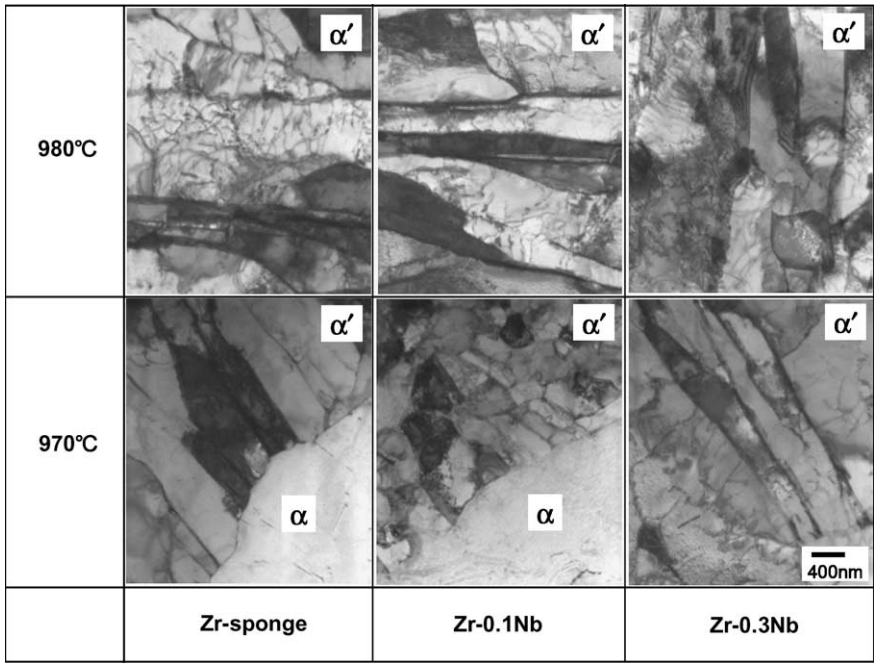

Fig. 4. TEM micrographs of Zr–*x*Nb alloys containing 1400 ppm O and 700 ppm Fe annealed at 970 °C and 980 °C.

temperatures of the $(\alpha + \beta)$ area were decreased with an increasing Nb content because Nb is the β stabilizing element. The transus temperatures with the Nb contents were not clearly defined in the DSC results due to the overheating effect on the incubation time of the diffusion controlled phase

transformation. However, the $\alpha/(\alpha+\beta)$ and $(\alpha+\beta)/\beta$ transformation range of the Zr–Nb system was roughly obtained by DSC results.

The phase equilibria of the alloys is characterized by the structural change which was observed by the optical microscope. Fig. 2 shows the optical micrographs of the Zr–xNb ($x = 0.0$–0.6 wt%) alloys annealed at 810–980 °C to investigate the $\alpha/(\alpha+\beta)$ and $(\alpha+\beta)/\beta$ transus lines of the Zr-rich region. The martensitic microstructure which had been initially formed by a fast cooling at the β phase region was changed with a variation of the annealing conditions and the Nb contents. After an isothermal annealing at various temperatures for a long time, the new microstructures such as the α and α′(prior β) phase were formed at some conditions. So, it is possible that the phase state of the alloys with various annealing temperatures and Nb contents could

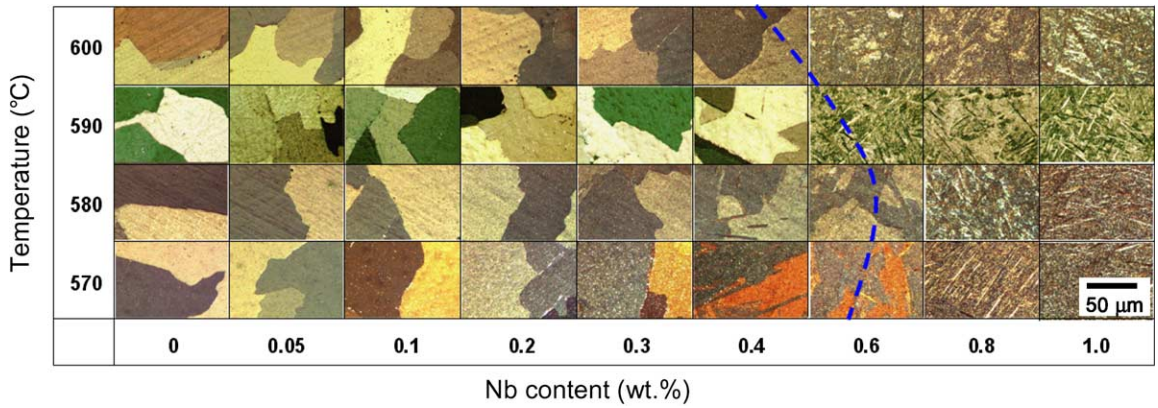

Fig. 5. Optical micrographs of Zr–xNb alloys containing 1400 ppm O and 700 ppm Fe annealed at various temperatures.

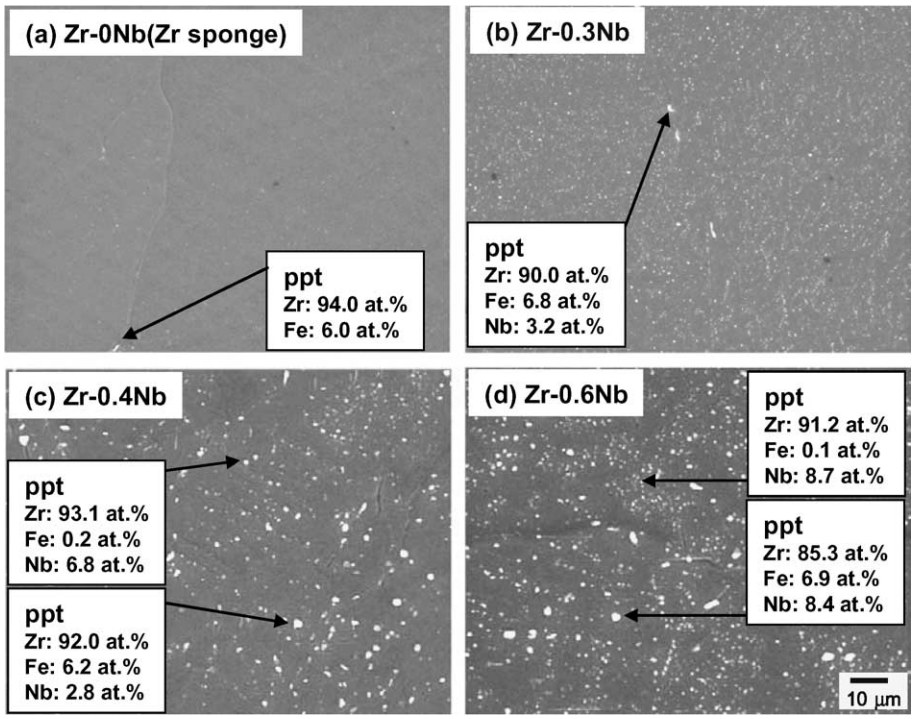

Fig. 6. SEM micrographs of Zr–xNb alloys containing 1400 ppm O and 700 ppm Fe annealed at 580 °C for 3 months.

be defined by a microstructural characterization. In the sponge Zr containing 1400 ppm O and 700 ppm Fe, the fully recrystallized α phase was observed by an annealing at 810 °C. And the mixed α and α′ (prior β) phase, and the α′ phase were observed at the annealing temperature at 820–970 °C, and 980 °C, respectively. These microstructural changes such as the α and α′ (prior β) phase were similarly observed in other Zr–*x*Nb alloys containing 1400 ppm O and 700 ppm Fe, and the $\alpha/(\alpha+\beta)$ and $(\alpha+\beta)/\beta$ transus temperatures were decreased with an increasing Nb content.

To clearly define the $\alpha/(\alpha+\beta)$ transus region, the SEM observation was performed for the sponge Zr at different annealing temperatures as shown in Fig. 3. The sponge Zr containing 1400 ppm O and 700 ppm Fe was found to have two-phase structures consisted of α and β when the annealing temperature was more than 820 °C, and the fraction of the β phase was increased by increasing the annealing temperature. Also the analysed Fe content in the β phase was decreased with an increasing annealing temperature. Fig. 4 shows the TEM micrographs of the Zr–*x*Nb ($x = 0.0$–0.3 wt%) alloys annealed at 970 °C and 980 °C. The mixed structure of the α and α′ phase and the single structure of the α′ phase were observed at the annealing temperatures of 970 °C and 980 °C, respectively. From these results of the OM, SEM, and TEM analysis, the $\alpha/(\alpha+\beta)$ and $(\alpha+\beta)/\beta$ transus temperatures for the sponge Zr containing 1400 ppm O and 700 ppm Fe were defined as 815 °C and 975 °C, respectively.

3.2. Nb solubility in α-Zr of quaternary alloy

Fig. 5 shows the optical micrographs of the Zr–*x*Nb ($x = 0.0$–1.0 wt%) alloys annealed at 570 °C to 600 °C to investigate the Nb solubility in α-Zr of quaternary alloy. The maximum composition at which the single recrystallized α phase is retained can be defined as the Nb solubility in α-Zr at a certain temperature. The alloys containing more Nb than the solubility were found to have the

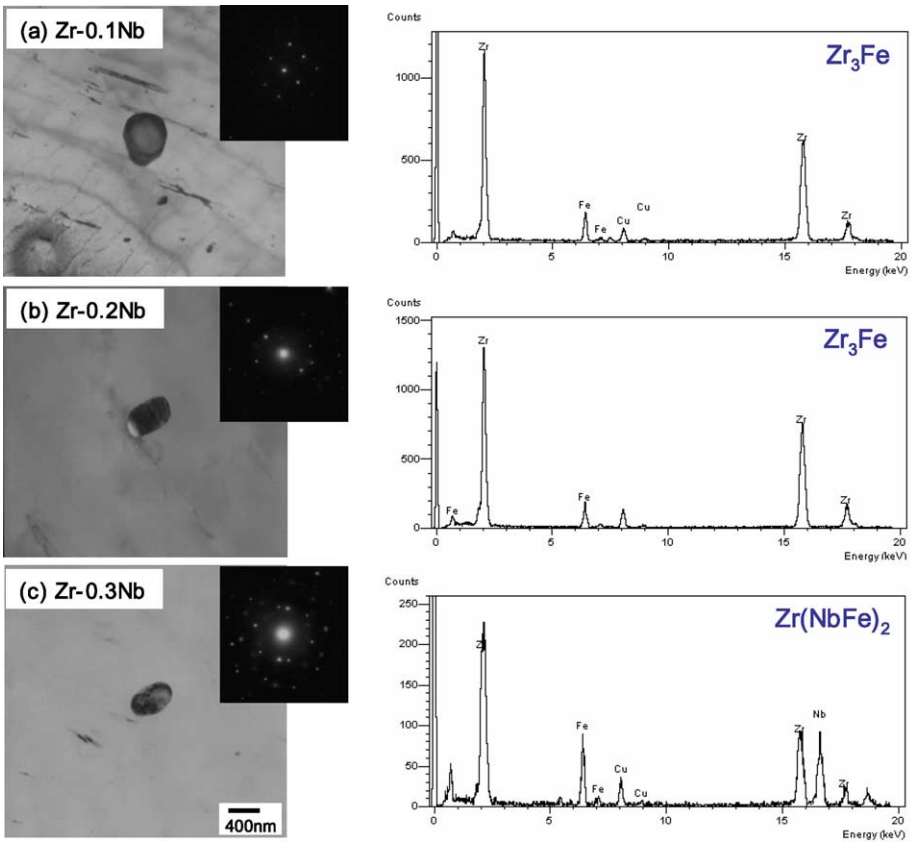

Fig. 7. TEM micrographs of Zr–*x*Nb alloys containing 1400 ppm O and 700 ppm Fe annealed at 580 °C for 3 months.

two-phase structure consisted of α and α′ after an annealing for a long time to get the equilibrium phase. It was shown that the α/α′ phase boundary in α-Zr increased to reach a maximum value at 580 °C and then decreased by increasing the temperature. From the observation of the optical micrographs, the Nb solubility in α-Zr could not clearly define because the Nb-containing precipitates which could determine the Nb solubility were not observed in the optical microstructure. Therefore, SEM and TEM analysis were performed to clearly investigate the formation of the Nb-containing precipitates.

Fig. 6 shows the SEM micrographs of the Zr–xNb ($x = 0.0$–0.6) alloys annealed at 580 °C. Very small Nb-containing precipitates were randomly distributed in the α grains as well as at the grain boundaries and their density increased by increasing the Nb contents. The composition of the precipitates was analyzed by EDS in SEM. Although the quantitative composition was not clearly defined by SEM–EDS analysis because the analyzed area by EDS was larger than the precipitate size, it is possible to assume that the Nb solubility in α-Zr would be below than 0.3 wt%.

Fig. 7 shows the TEM micrographs and EDS spectra for the precipitates of the Zr–xNb ($x = 0.1$, 0.2 and 0.3) alloys. It was observed that the precipitates in the Zr–0.1Nb and Zr–0.2Nb alloys consisted of Zr and Fe from the EDS reaults, while the precipitates in the Zr–0.3Nb alloy consisted of Nb as well as Zr and Fe. The precipitates type in the Zr–xNb alloys was reported in a previous study [16]. The Fe containing precipitate originated from the Fe contained in the sponge Zr because the Fe content (700 ppm) in all the tested samples was much higher than the Fe solubility in α-Zr (about 100 ppm). Although the β phase was not observed in the analyzed alloys (to 0.3 wt% Nb), it was frequently observed in the Zr–0.6Nb alloy. It is suggested that 0.3Nb was higher than the Nb solubility in α-Zr of quaternary alloy because the Nb was precipitated in the second phase. It should be considered that the Nb solubility in α-Zr was affected by an element such as Fe which is known as one of the β stabilizers. Consequently, the Nb solubility in α-Zr of quaternary alloy was determined to be 0.2 wt% because the Nb containing precipitates were not found in the analysed specimens contained up to 0.2 wt% Nb of the alloys. The Nb solubility in α-Zr obtained by the TEM observation was clearly showed compared with the result from the OM observation.

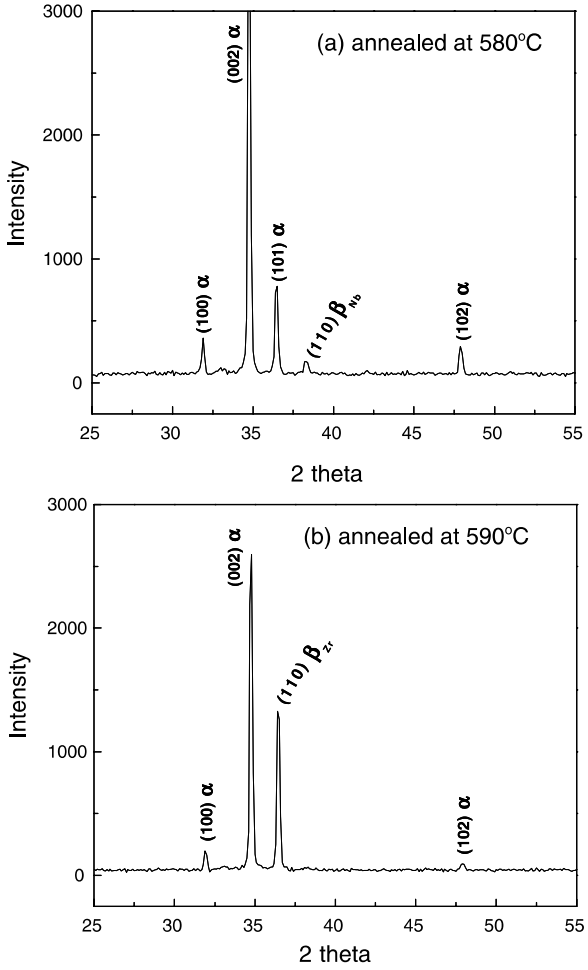

Fig. 8. XRD spectra of Zr–2.0Nb alloys containing 1400 ppm O and 700 ppm Fe annealed at (a) 580 °C and (b) 590 °C for 3 months.

3.3. Monotectoid temperature in the Zr–Nb system

In order to determine the monotectoid temperature in the Zr–Nb system containing 1400 ppm O and 700 ppm Fe, the sheets of Zr–2.0Nb alloy were annealed at the temperature of 580 °C and 590 °C for 1500 h to get the full equilibrium state.

Fig. 8 shows the XRD spectra of the Zr–2.0Nb alloy annealed at 580 °C and 590 °C. The peaks of the α-Zr phase were found for both the alloys annealed at different temperatures. The peak of the β-Nb phase was found in the specimen annealed at 580 °C while that of the β-Zr phase was found in the specimen annealed at 590 °C. It can be suggested that the phase transformation from the β-Nb to the β-Zr phase occurred between 580 °C and 590 °C.

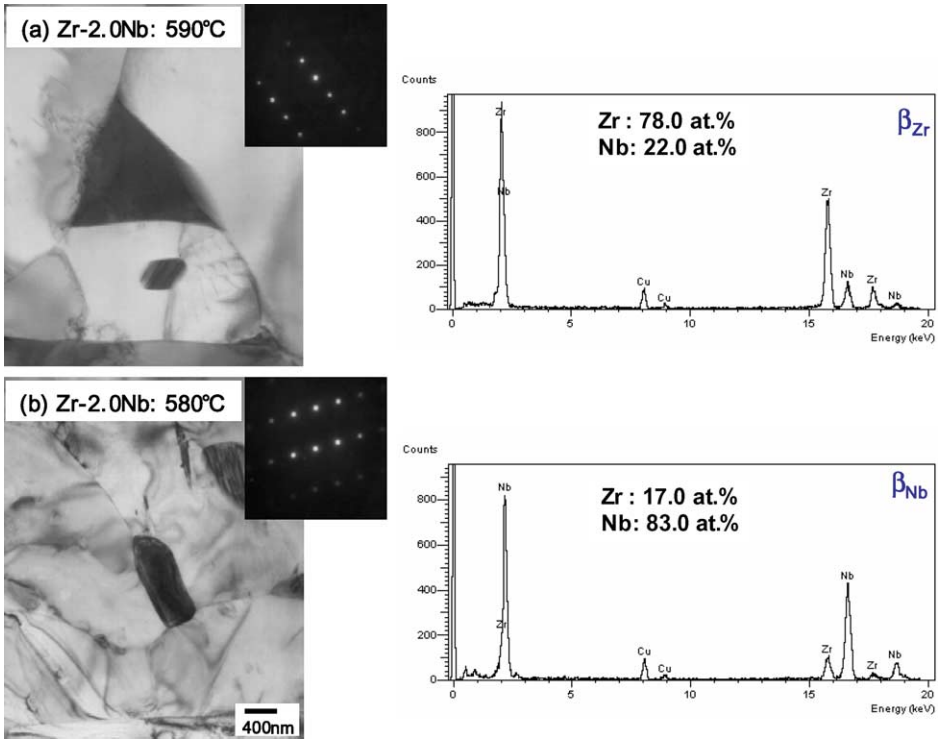

Fig. 9. TEM micrographs of Zr–2.0Nb alloys containing 1400 ppm O and 700 ppm Fe annealed at (a) 580 °C and (b) 590 °C for 3 months.

Fig. 9 shows the TEM microstructures and EDS spectra for the constituent phases of the Zr–2.0Nb alloy annealed at different temperatures of 580 °C and 590 °C. In the EDS data, the Cu peak resulted from the Cu holder which was used for the TEM specimen fixing. The chemical analyses by the EDS revealed that the β-Zr phase (Nb ≈ 20 wt%) was formed in the specimen annealed at 590 °C while the β-Nb phase (Nb ≈ 80 wt%) was formed in the specimen annealed at 580 °C. This result was consistent with the XRD result. The crystal structure of the β-Zr and β-Nb phase was identified as a BCC structure from the diffraction pattern analysis. From the results obtained from the XRD and TEM observations, the monotectoid temperature of the commercial grade Zr–Nb alloy containing 1400 ppm O and 700 ppm Fe would be approximately 585 °C. This monotectoid reaction temperature was slightly different to that in a recent study which showed a monotectoid temperature of about 600 ± 5 °C in Zr–1%Nb (~1200 wt% oxygen) [17].

3.4. Phase boundary of the Zr–Nb system

The phase boundary of the Zr-rich region in the Zr–Nb system was established from the results obtained using the sponge-type Zr containing 1400 ppm O and 700 ppm Fe. Fig. 10 shows the phase boundary of the Zr-rich region in a restricted quaternary alloy of Zr–0.14O–0.07Fe–*x*Nb system as a function of the temperature and Nb content. The detailed microstructures for a critical area are exhibited in Fig. 2 showing the $\alpha/(\alpha+\beta)$ and $(\alpha+\beta)/\beta$ transus temperatures, and Fig. 5 showing the maximum α region. On the basis of the microstructural observation using OM in this study, it is possible that the phase boundary in a commercial grade Zr–Nb containing 1400 ppm O and 700 ppm Fe could be roughly determined. The published results [7–13] for the phase boundary of Zr–Nb alloy were somewhat differently reported because it would be affected by the experimental method or impurity contents. Although the Nb solubility in α-Zr of quaternary Zr–Nb system containing 1400 ppm O and 700 ppm Fe could not be determined from the optical micrographs shown in Fig. 5, it was clearly determined from the results of the SEM and TEM chemical analysis for the precipitates shown in Figs. 6 and 7.

The Nb solubility in α-Zr at the monotectoid temperature should be carefully determined because the phase characteristics depend on the applied

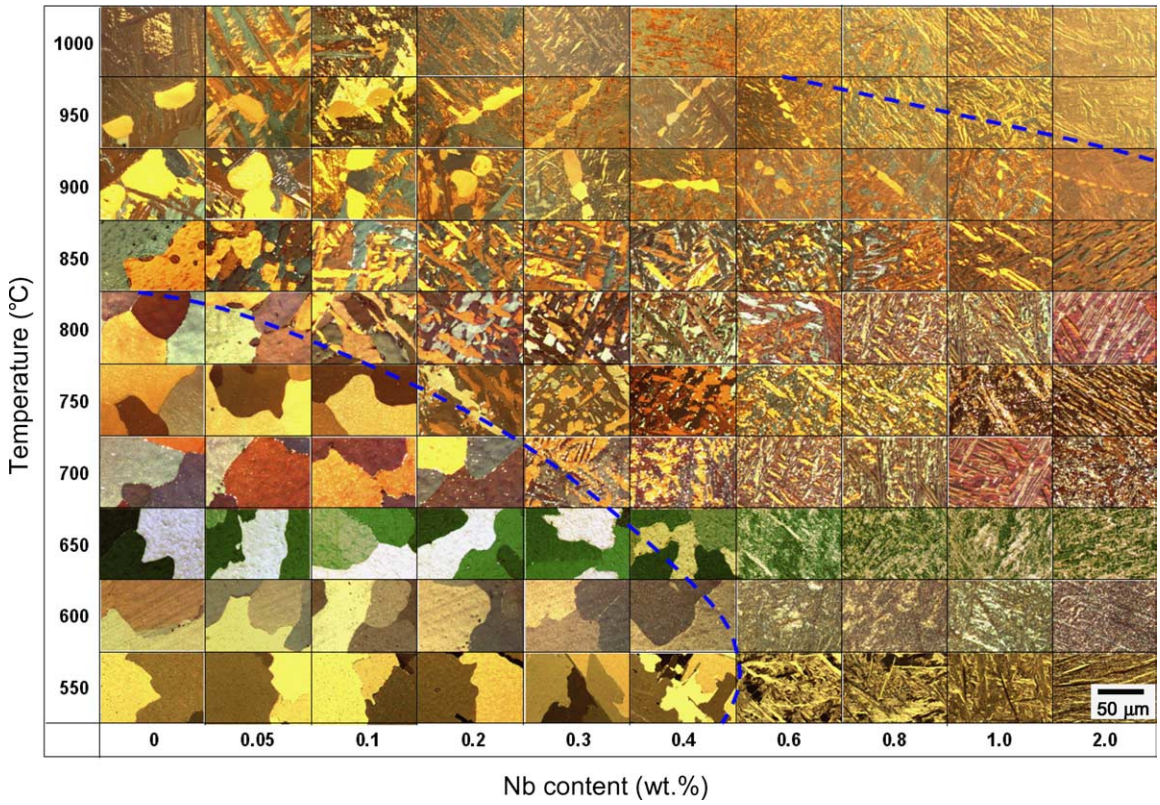

Fig. 10. Optical micrographs of Zr–*x*Nb alloys containing 1400 ppm O and 700 ppm Fe annealed from 550 to 1000 °C.

experimental methods and impurity contents. In the optical microstructure characteristics for the α/α′ phase boundary, the critical change of the grain morphology was observed between 0.4 and 0.6 wt% Nb. But the Nb-containing precipitates which could determine the Nb solubility were not observed in the optical microstructure. Therefore, it is suggested that the microstructure observation using optical microscopy was not suitable to determine the Nb solubility in α-Zr.

Fig. 11 shows the phase boundary of the Zr-rich region determined by various experimental methods in this study. The Zr–Nb alloy used in this study could not be defined as the real binary system because Zr material containing 1400 ppm O and 700 ppm Fe was used. Therefore, the result of the phase boundary determination in this study was somewhat different from that of the phase boundary determination reported for the Zr–Nb binary alloy, but this phase boundary of the pseudo binary alloy is more useful for the development of advanced Zr alloys which usually contain O and Fe of a 10^2–10^3 ppm level.

From this study, it was found that the (α + β)/β transformation temperature of the commercial grade Zr system containing 1400 ppm O and 700 ppm Fe was 970 ± 3 °C and the α/(α + β) transformation temperature was 815 ± 3 °C. The temperature change of the (α + β)/β phase boundary of Zr–Nb alloy was attributed to the O concentration [15,18]. On the contrary, the α to (α + β) phase transformation temperature of the sponge Zr was lower than that of the iodide Zr, which could have resulted from a high Fe content that acted as β stabilizer as shown in Fig. 3. The combination effect of O and Fe would be expanded the (α + β) two phase region of the Zr–Nb pseudo-binary system. The Nb solubility in α-Zr and the monotectoid temperature of quaternary alloy was determined as 0.2 wt% and 585 ± 3 °C, respectively. It could be suggested that the Nb solubility was affected by the high Fe content in the sponge Zr. It was also found that a ternary intermetallic phase such as a ZrNbFe-type precipitate was formed in the commercial grade Zr–Nb alloys as shown in Fig. 7. Therefore, the Nb solubility of this system was lower than that of

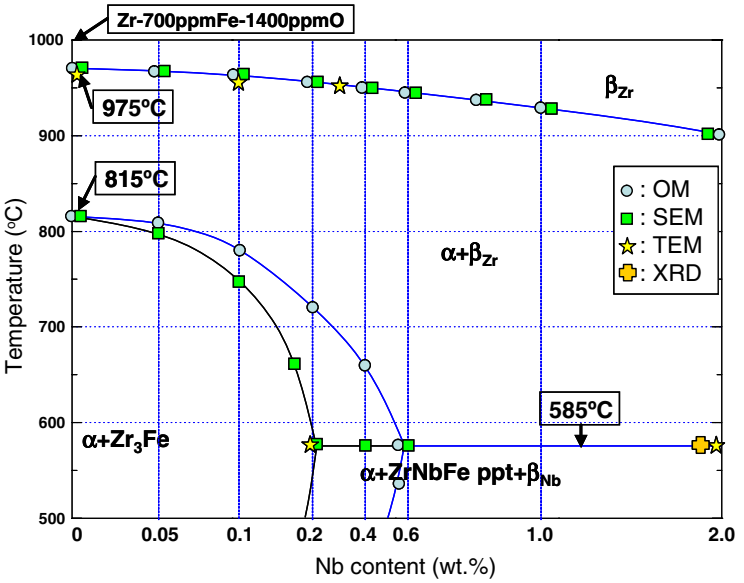

Fig. 11. Phase boundary determination of dilute Zr–*x*Nb alloys containing 1400 ppm O and 700 ppm Fe.

the iodide Zr–Nb alloy. It is concluded that the O and Fe contained in sponge Zr plays a critical role in expanding the $(\alpha + \beta)$ region and decreasing the Nb solubility in α-Zr and the monotectoid temperature when compared with the Zr–Nb alloy made from the iodide Zr.

4. Conclusions

The phase boundary of $\alpha/(\alpha + \beta)$ and $(\alpha + \beta)/\beta$, the Nb solubility in α-Zr, and the menotectoid temperature in the Zr-rich region of the Zr–0.14O–0.07Fe–*x*Nb quaternary system were investigated using DSC, OM, SEM, TEM and XRD. The sponge-type Zr–Nb alloys containing 1400 ppm O and 700 ppm Fe which are usually contained in commercial fuel cladding materials were used to determine the phase boundary. The $\alpha/(\alpha + \beta)$ and $(\alpha + \beta)/\beta$ transus temperatures for the sponge-type commercial grade Zr were defined as 815 ± 3 °C and 975 ± 3 °C, respectively. The Nb solubility in α-Zr of quaternary alloy was determined to be 0.2 wt% obtained by the TEM–EDS analysis. In addition, the monotectoid temperature of the Zr–Nb alloy would be approximately 585 ± 3 °C from the results of the XRD and TEM observation. From this study, the phase boundary of the Zr-rich region was established for the Zr–Nb alloy manufactured using the commercial grade Zr and the high purity Nb. It is concluded that the O and Fe contained in the commercial grade Zr–Nb alloys plays a critical role in expanding the $(\alpha + \beta)$ region and decreaseing the Nb solubility in α-Zr and the monotectoid temperature when compared to previous results using a high purity Zr.

Acknowledgements

This study was supported by Korea Institute of Science and Technology Evaluation and Planning (KISTEP) and Ministry of Science and Technology (MOST), Korean government, through its national nuclear technology program.

References

[1] G.P. Sabol, G.R. Kilp, M.G. Balfour, E. Roberts, ASTM STP 1023 (1989) 227.
[2] A.V. Nikulina, A.M. Vladimir, M.M. Peregud, Y.K. Bibilashvili, V.A. Kotrekhov, A.F. Lositsky, N.V. Kuzmenko, Y.P. Shevnin, V.K. Shamardin, G.P. Kobylyansky, A.E. Novoselov, ASTM STP 1295 (1996) 785.
[3] J.-P. Mardon, D. Charquet, J. Senevat, ASTM STP 1354 (2000) 505.
[4] J.Y. Park, Y.H. Jeong, Y.H. Jung, Met. Mater. Inter. 7 (2001) 447.
[5] G.P. Sabol, R.J. Comstock, R.A. Weiner, P. Larourer, R.N. Stanutz, ASTM STP 1245 (1994) 724.
[6] V.F. Urbanic, M. Griffiths, ASTM STP 1354 (2000) 641.
[7] C.E. Lundin, R.H. Cox, USAEC Report, GEAP-4089 1, 1962, pp. 9.
[8] H. Richter, P. Wincierz, K. Anoerko, U. Zwicker, J. Less-Common Met. 4 (1962) 265.

[9] O.S. Ivanov, V.K. Grigorovich. In: Proc. of the 2nd UN International Conf. on the Peaceful Uses of Atomic Energy, Vol. 5, 1958, p. 34.
[10] E.S. Hodge, USAEC Report, TID-5061, 1952, pp. 461.
[11] B.A. Rogers, D.F. Atkins, Trans. AIME 203 (1955) 1034.
[12] Y.F. Bychkov, A.N. Rozanov, D.M. Skorov, J. Nucl. Energ. 5 (1957) 402.
[13] Bethune, Williams, J. Nucl. Mater. 29 (1969) 129.
[14] Abriata, Bolcich, Bull. Alloy Phase Diagrams 3 (1) (1982).
[15] D.O. Northwood, D.C. Gillies, Microstruct. Sci. 7 (1979) 123.
[16] Y.H. Jeong, H.G. Kim, T.H. Kim, J. Nucl. Mater. 317 (2003) 1.
[17] C. Toffolon, J.-C. Brachet, C. Servant, L. Legras, D. Charquet, P. Barberis, J.-P. Mardon, ASTM STP 1423 (2002) 361.
[18] C.E.L. Hunt, P. Niessen, J. Nucl. Mater. 35 (1970) 134.